Available online at www.sciencedirect.com
ScienceDirect
Journal of Catalysis 245 (2007) 348–357
JOURNAL OF CATALYSIS
www.elsevier.com/locate/jcat

Effect of alkali additives over nanocrystalline Co–Cu-based perovskites as catalysts for higher-alcohol synthesis

Nguyen Tien-Thao [a], M. Hassan Zahedi-Niaki [a], Houshang Alamdari [b], Serge Kaliaguine [a,*]

[a] *Department of Chemical Engineering, Laval University, Quebec, G1K 7P4 Canada*
[b] *Nanox Inc., 4975 Rue Rideau, Quebec, G2E 5H5 Canada*

Received 17 July 2006; revised 9 October 2006; accepted 21 October 2006

Available online 28 November 2006

Abstract

A series of $LaCo_{0.7}Cu_{0.3}O_{3-\delta}$ perovskites prepared by mechano-synthesis using different alkali additives was characterized by several techniques (AAS, BET, XRD, H_2-TPR) and tested under typical higher-alcohol synthesis conditions. Using group I elements as additives allowed substantial enhancement of the specific surface area of nanocrystalline $LaCo_{1-x}Cu_xO_{3-\delta}$ perovskites. The catalyst surface area varied with the cationic radius of the alkali metal used. The perovskite precursors were prereduced in situ at 500 °C under flowing H_2/Ar, providing copper/cobalt metals dispersed over an oxide support, La_2O_3. Reaction tests were carried out at 275 °C, 1000 psi, VVH = 5000 h^{-1}, and H_2/CO/He = 8/4/3. The products included paraffins, olefins, normal alcohols, and carbon dioxide. The alkali ions remaining on the surface of the reduced $LaCo_{0.7}Cu_{0.3}O_{3-\delta}$ perovskite had a strong influence on the CO conversion, WGS reaction, selectivity, and alcohol and hydrocarbon productivity. An optimum content of alkali promoter in this study was in the range of 0.1–0.3 wt%. The promotional effect of such alkali metals on CO hydrogenation was to improve the propagation of the hydrocarbon chain of both hydrocarbons and alcohol products. The carbon number distributions of normal alcohols and hydrocarbon products were consistent with the ASF plot. The chain growth probability factors of products were correlated with the alkali electronegativity. Alcohol selectivity was in the range of 25.7–48.9%. Alcohol productivity was strongly dependent on the presence and content of residual alkali additives and on reaction temperature. The presence of an alkali promoter was necessary for higher-alcohol synthesis from syngas.

Keywords: Alkali; Promoter; Higher alcohol; Syngas; $LaCoCuO_3$; Co–Cu metals

1. Introduction

Perovskites have been known as catalysts and catalyst precursors for conversion of syngas to many useful chemicals and liquid fuels [1–3]. These oxide materials can produce a highly dispersed metal phase under controlled reduction condition and/or transform into active phases when exposed to synthesis gas at typical reaction temperatures [3,4]. For example, $LaCoFeO_3$ perovskite-type mixed oxides have been widely adopted catalysts for Fischer–Tropsch synthesis [2,3]. Mn–Cu-based perovskites have been proposed for alcohol synthesis from syngas [1]. $LaRhO_3$ catalyst has been used for the hydrogenation of carbon monoxide at relatively low pressure (6 atm) and temperature (225–375 °C), giving a large yield of oxygenated compounds (up to 80 wt%) [5].

Under various experimental conditions, several phases, including metals, carbides, and lower oxides (MO_x), have been proposed as active centers for syngas conversion. A number of components, including oxides (e.g., ZnO, CuO), metals (e.g., Rh, Ru, Cu), and alkali (e.g., Na, K, Rb, Cs) ions, have been introduced into catalysts as promoters to improve their physical and chemical catalytic properties [1,3,5–9]. In general, potassium as a promoter affects CO conversion and improves selectivity toward higher-molecular weight products [10–13]. In the absence of potassium, a large amount of methane is favored over Fischer–Tropsch catalysts from syngas [13–15]. Furthermore, higher alcohols can become major products if a proper promoter is used. Such characteristics have led to the appearance of several higher-alcohol catalyst systems developed by

* Corresponding author. Fax: +1 (418) 656 3810.
E-mail address: serge.kaliaguine@gch.ulaval.ca (S. Kaliaguine).

0021-9517/$ – see front matter
doi:10.1016/j.jcat.2006.10.026

modifying Fischer–Tropsch catalysts [14,16–18]. The presence of alkali promoter on Fischer–Tropsch catalysts could in some cases result in either acceleration or inhibition of the reaction rate of CO conversion, although the influence of such a promoter on catalytic activity remains unclear [12,16,19–21].

In practice, the role of alkali metal can be manifested in two major ways: improvement in selectivity and/or activity and prolongation of the effective lifetime. In Fischer–Tropsch synthesis, the relative activity of catalysts containing an equal atomic amount of alkali promoters increases in the order Li < Na (≈Rb) < K [12,13]. However, the catalytic activity not only is dependent on the basicity of alkali ions added, but also is related to the counter anion of the salt used and the nature of the supports [6,11,22]. The acidic supports (e.g., silica, Cr_2O_3, Al_2O_3) usually require higher amounts of promoter to obtain the desired selectivity spectrum [11,13,15,21]. Therefore, introduction of an optimum amount of alkali into a Fischer–Tropsch catalyst results in increased average molecular weight and olefin-to-paraffin ratio of products, increased water–gas shift (WGS) activity, and strong suppression of CH_4 production [9,11,12]. Furthermore, addition of alkali metals to both low-temperature (e.g., CuO/ZnO, CuO/ZnO/Al_2O_3) and high-temperature methanol synthesis catalysts (e.g., ZnO/Cr_2O_3) could steer the behavior of such methanol synthesis catalysts toward production of higher alcohols in addition to methanol in many cases [7,15,20].

With the exception of cesium, the effect of alkali doping on both types of catalysts has in practice decreased the selectivity to methanol by converting this product to higher alcohols [15, 20,22]. Cesium is reported to be the best promoter for branched higher alcohol synthesis on the methanol synthesis catalysts [7, 15,20–22], but it is much less effective for linear primary alcohols over the modified Fischer–Tropsch catalysts, whereas Li, Na, and K are more effective for primary higher-alcohol production [14,16,18,19,23]. The function of alkali metals is to neutralize the surface acidity that catalyzes various undesired reactions, and also to facilitate adsorption of CO molecules on the catalyst surface [15,16,20,22,23]. In Co–Cu-based alcohol synthesis catalysts, doping with alkali promoters results in substantial improvement in C_2^+OH selectivity, as well as strong suppression of methane formation through modification of Co–Cu active sites [19,23–25]. Nunan et al. [15,25] reported that cesium dopant significantly enhanced the synthesis of methanol and higher alcohols over CuO/ZnO and Cu/ZnO/M_2O_3 catalysts (M = Al, Cr). The productivity of alcohols passed through distinct maxima at cesium nominal concentrations of 0.3–0.5%. In this case, the principal effects of cesium were reported to inhibit synthesis of dimethyl ether, improve ethanol synthesis, and enhance ethanol conversion to *n*-propanol and subsequently to higher alcohols (particularly 2-methyl-1-propanol).

Unlike alkali-promoted copper-zinc oxide catalysts [15,20, 25], which mainly promote the production of isobutanol, the modified Fischer–Tropsch catalysts (CuO/CoO/Al_2O_3) doped with alkali have different effects on activity. De Aquino and Cobo [23] observed that the addition of K in an Al–Co–Cu catalyst resulted in decreased higher-alcohol (C_3^+OH) and hydrocarbon productivities at 250 °C (5 MPa, $H_2/CO = 2$), whereas addition of cesium drastically reduced the productivity of all alcohols, alkanes, and alkenes. In contrast, the addition of lithium dopant led to an increase in the selectivity toward higher alcohols, whereas addition of sodium had an unclear promotional effect on alcohol production [23]. Meanwhile, Dalmon et al. [16] reported a modest increase in higher alcohol selectivity (∼6%) over Al–Co–Cu–Na catalysts under similar conditions. Therefore, the ability of group IA elements to promote higher-alcohol synthesis has not been fully elucidated.

In a previous report [26], we presented a set of $LaCo_{1-x}Cu_xO_{3-\delta}$ perovskites acting as higher-alcohol synthesis catalysts. These were prepared by the reactive grinding technique, which allows rather high specific surface areas of the perovskite precursor and a higher reducibility of the fraction of both Co and Cu ions located in the grain boundaries. Both properties are thought to be beneficial for the catalytic performance in higher-alcohol synthesis. The purpose of the present work is to study the promotional effects of alkali elements over $LaCo_{1-x}Cu_xO_{3-\delta}$ perovskites prepared by reactive grinding on their catalytic activity in higher-alcohol synthesis from syngas.

2. Experimental

2.1. Perovskite preparation

$LaCo_{0.7}Cu_{0.3}O_{3-\delta}$ perovskite-type mixed oxides were synthesized by high-energy ball milling as described previously [26,27]. The stoichiometric proportions of commercial lanthanum, copper, and cobalt oxides (99%, Aldrich) were blended together with three hardened steel balls (diameter = 11 mm) in a hardened steel crucible (50 mL). A SPEX high-energy ball mill operating at 1000 rpm was used for mechano-synthesis. Milling was carried out for 8 h before a second milling step with additives. Then the resulting powder was mixed to 50% alkali chloride (99.9%) and further milled under the same conditions for 12 h before the additives were washed with distilled water. A sample was added into a beaker containing 800 mL of water and stirred by magnetic stirring for 90 min before being sedimented for 3–5 h, followed by decantation. This was performed to remove the additive. The slurry was dried in oven at 60–80 °C before a series of successive further washing steps. Finally, all samples were calcined for 3 h in air at both 200 and 500 °C. Both series were submitted to N_2 adsorption isotherm measurement; only the series calcined at 500 °C was prereduced and submitted to catalytic tests. The $LaCo_{0.7}Cu_{0.3}O_{3-\delta}$ samples are designated as X*i* = Li*i*, Na*i*, K*i*, Rb*i*, and Cs*i* (where *i* refers to the number of successive washing operations), corresponding to the additives LiCl, NaCl, KCl, RbCl, and CsCl (Table 1).

A reference sample without any alkali promoter, $LaCo_{0.7}Cu_{0.3}O_{3-\delta}$ (designated as NAl), was prepared by the conventional citrate method [1]; a stoichiometric amount of $La(NO_3)_3$ was added into distilled water while the mixture was slowly heated on a magnetic stirrer. Once a clear transparent solution was obtained, stoichiometric amounts of cobalt and copper nitrates were added. Then 1 mole of citric acid per mole of metal atom was added to the dark-pink/red translucent solution. The

Table 1
Physical properties of $LaCo_{0.7}Cu_{0.3}O_{3-\delta}$

Sample (X*i*)	Additive	S_{BET} (m^2/g)[a]	S_{BET} (m^2/g)[b]	Composition (wt%)			
				Alkali+	Co	Fe[c]	Cu
Li1	LiCl	13.6	8.6	0.12	15.39	1.02	5.39
Li2		15.8	9.1	0.04	16.79	1.04	5.17
Li3		16.9	9.8	0.01	15.38	1.01	5.28
Na1	NaCl	25.2	14.7	0.63	16.32	0.85	5.42
Na2		25.3	14.5	0.08	16.30	0.83	5.16
Na3		25.7	14.9	0.06	16.15	0.86	5.31
K1	KCl	29.0	17.8	0.75	16.86	0.67	5.84
K2		34.5	26.2	0.1	16.02	0.63	5.44
K3		37.0	30.6	0.05	16.30	0.64	5.65
Rb1	RbCl	34.6	19.2	0.61	16.24	0.98	5.58
Rb2		46.3	31.0	0.09	15.76	0.95	5.32
Rb3		46.8	34.7	0.03	15.68	0.97	5.52
Cs1	CsCl	25.6	23.2	0.75	15.65	0.85	5.69
Cs2		26.1	23.3	0.15	16.32	0.87	5.27
Cs3		27.4	24.0	0.08	15.74	0.84	5.79

[a] Calcined at 200 °C.
[b] Calcined at 500 °C.
[c] Iron impurity from mechano-synthesis.

resulting solution was heated slowly to dryness and then dehydrated at 383 K overnight in a vacuum oven to yield an amorphous solid precursor. The sample was calcined at 800 °C for 6 h with a ramp of 3 °C/min under air.

2.2. Characterization

The chemical analysis (Fe, Co, Cu) of the perovskites and the residual impurities was performed by atomic absorption spectroscopy using a Perkin–Elmer 1100B spectrometer. Before each analysis, a weighed amount of sample was digested in a 10% HCl solution at 60–70 °C overnight. The specific surface area of all obtained samples was determined by nitrogen adsorption equilibrium at −196 °C using an automated gas sorption system (NOVA 2000; Quantachrome). Then 300–500 mg of each sample was degassed at 200 °C for 6–7 h to remove the humidity before N_2 adsorption measurements.

Phase analysis and particle size determination were performed by powder X-ray diffraction (XRD) using a Siemens D5000 diffractometer with Cu$K\alpha$ radiation ($\lambda = 1.54059$ nm). Bragg's angles between 15° and 65° were collected at a rate of 1°/min. Average particle sizes (D) were evaluated by means of the Debye–Scherrer equation, $D = K\lambda/\beta\cos\theta$, after Warren's correction for instrumental broadening [28]. Here K is a constant equal to 0.89; λ is the wavelength of the X-ray used; β is the effective line width of the X-ray reflection under observation, calculated by the equation $\beta^2 = B^2 - b^2$ (in which B is the full width at half-maximum [FWHM], b is the instrumental broadening determined through the FWHM of the X-ray reflection at $2\theta \approx 28°$ of SiO_2 with particles larger than 1000 Å); and θ is the diffraction angle of the plane considered to be X-ray reflection.

Temperature-programmed reduction (TPR) experiments were carried out using a flow system with a multifunctional catalyst testing and characterization apparatus (Advanced Scientific Designs RXM-100). The reactor was connected to a thermal conductivity detector (TCD). Before each TPR analysis, a 40–80 mg sample was calcined at 500 °C for 90 min under flowing 20% O_2/He (20 ml/min, ramp 5 °C/min). Then the sample was cooled to room temperature under flowing pure He (20 mL/min). TPR of the catalysts was then carried out by ramping under 4.65 vol% of H_2/Ar (20 ml/min) from room temperature up to 800 °C (5 °C/min). The hydrogen consumption was determined using a TCD with a reference gas of the same composition as the reducing gas (H_2/Ar). The effluent gas was passed through a cold trap (dry ice/ethanol) to remove water before detection.

2.3. Catalytic performance

The catalytic tests were carried out in a stainless-steel continuous fixed-bed flow microreactor (BTRS-Jr PC, Autoclave Engineers). The reaction pressure was controlled using a backpressure regulator. The syngas mixture (H_2/CO = 2/1, Praxair) was diluted in 20 vol% helium. The mixture of reactants and inert gas was supplied from a pressurized manifold via individual mass flow controllers. The catalyst pellet size was 40–60 mesh. Catalysts were pretreated in situ under flowing 5 vol% of H_2/Ar (20 ml/min) before each reaction test. The temperature was kept at 250 °C for 3 h and at 500 °C for 3 h, with a ramp of 2 °C/min. Then the reactor was cooled to the reaction temperature while pressure was increased to 1000 psi by feeding inert gas before switching to the reaction mixture. Butane/helium (4.98 vol%) was used as an internal calibration standard. The products were analyzed using a gas chromatograph equipped with two capillary columns and an automated on-line gas sampling valve maintained at 170 °C. The temperature of the transfer line between the reactor and the valves was kept at 220 °C to avoid any product condensation. Carbon monoxide and carbon dioxide were separated using a capillary column (Carboxen™ 1006 PLOT, 30 m × 0.53 mm) connected to the TCD. Quantitative analysis of all organic products was carried out using the second capillary column (Wcot fused silica, 60 m × 0.53 mm; coating, Cp-Sil 5CB; DF = 5.00 μm) connected to a flame ionization detector (Varian CP-3800) and a mass spectrometer (Varian Saturn 2200 GC/MS/MS).

3. Results

3.1. Specific surface area

Table 1 summarizes the composition and BET specific surface area data for several perovskite samples. The surface area of ground perovskites varied with the size of alkali metals. Apart from the sample with Cs additive, the BET area of all samples increased monotonically with increasing cationic radius of alkali additives (Fig. 1). As discussed previously [26,27], alkali salt introduced into the mill during perovskite synthesis caused a partial separation of crystal domains, a decrease in grain size, and enhancement of specific surface area. The ground perovskites were composed mainly of nanoparticles

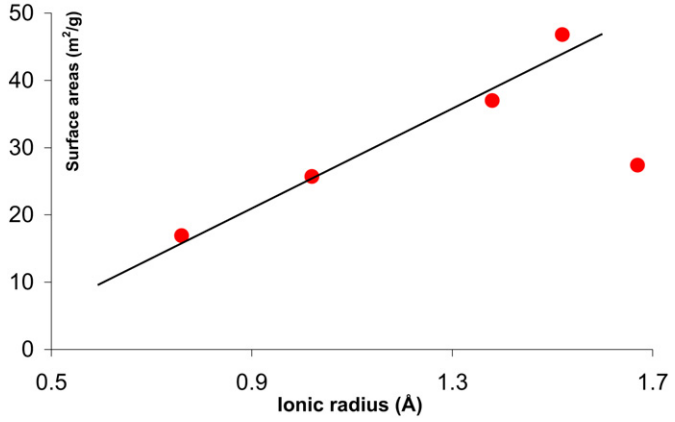

Fig. 1. The relationship between cationic radius of alkali additives and perovskite surface area after three successive washing steps.

[26,27,29–32]. There were many slit-shaped spaces between nanoparticles or micropores with pore diameters of 10–30 Å, as calculated from the adsorption/desorption isotherm data (Fig. 2). After the first washing step, the ground products still retained 0.12–0.75 wt% of the alkali metals, believed to be located between the grains and block part of the small slit-shaped spaces. Two further leaching operations almost completely removed the residual additives in the slit-shaped spaces, yielding a higher surface area. Fig. 2 shows the increase in specific surface area after three successive washings for two representative samples, K and Rb. Simultaneously, the smaller micropores were liberated from the blockage of alkali additives, as indicated by the changes in BJH pore size distribution for the K samples [32]. No significant difference in surface area was observed between samples Rb2 and Rb3, indicating that additives were almost completely leached out of the catalyst after two washings. The residual alkali ions were <0.08 wt% after the third washing (samples Li3–Cs3 in Table 1).

3.2. X-ray diffraction

The crystalline phase of catalysts was determined by powder XRD. The XRD patterns in Fig. 3 show well-formed perovskite structures. Minor crystalline impurities (CuO, Co_3O_4; JCPDS Nos. 41-1467 and 44-0706) were found, especially in sample Cs2, which may explain the anomalous BET surface area of this sample (Fig. 1) [26,33,34]. Both the d spacing (2.72–2.73 Å) and diffraction angle ($2\theta \approx 32.8°$) observed in XRD spectra of the present samples (Li2–Cs2) were close to those of patterns N2–N3 ($LaCo_{1-x}Cu_xO_{3-\delta}$, $x \approx 0.2$ and 0.3)

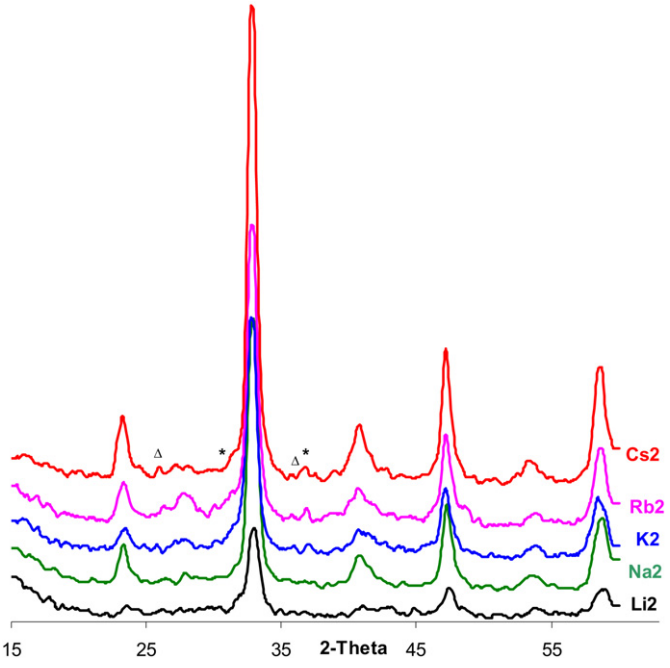

Fig. 3. Powder X-ray diffraction patterns X2 of $LaCo_{0.7}Cu_{0.3}O_{3-\delta}$ (△: Co_3O_4, ⋆: CuO).

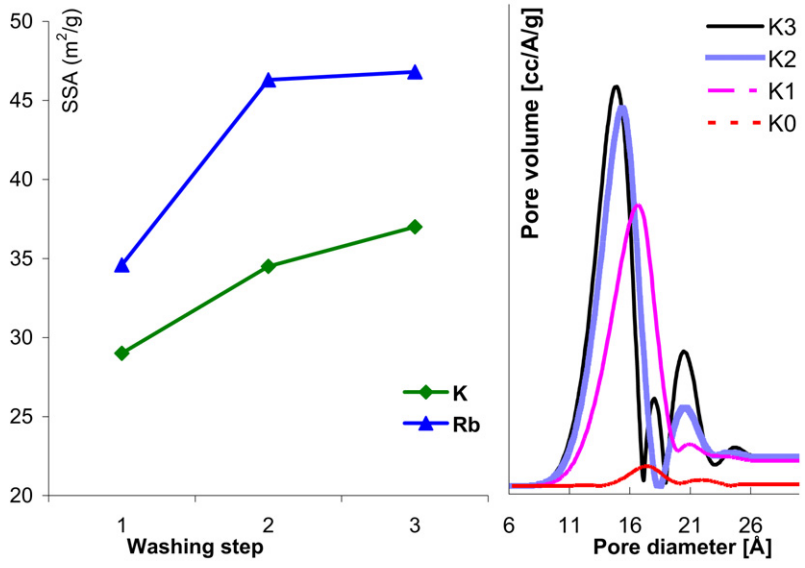

Fig. 2. BET surface area and BJH pore size distribution for K- and Rb-samples calcined at 200 °C (K0 is synthesized potassium-sample before any washing, $S_{BET} = 1.2\ m^2/g$).

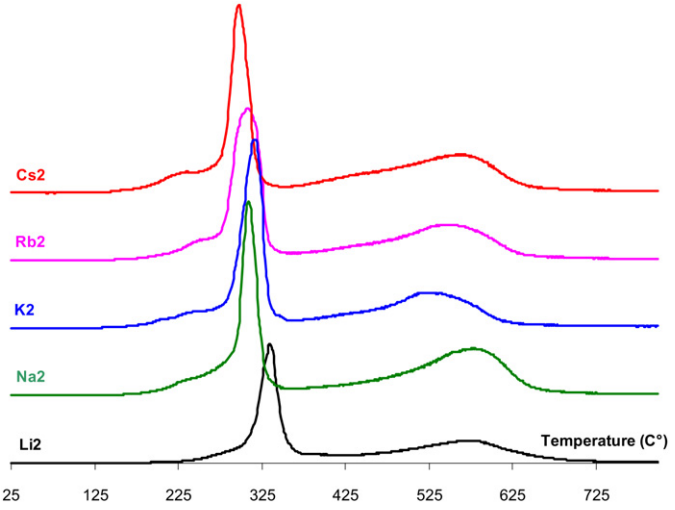

Fig. 4. Temperature-programmed reduction profiles of $LaCo_{0.7}Cu_{0.3}O_{3-\delta}$ samples X2.

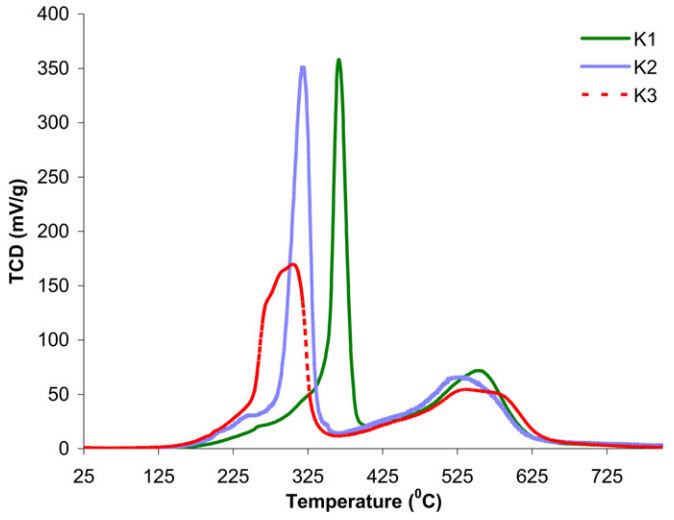

Fig. 5. H_2-TPR profiles of $LaCo_{0.7}Cu_{0.3}O_{3-\delta}$ samples K1–K3.

observed previously [26], indicating the successful substitution of Co with Cu in the perovskite lattice [33,34]. Even though alkali additives were determined by AAS (Table 1), no significant reflection lines of such compounds are seen in Fig. 3. All samples show well-crystallized perovskite with rhombohedral structure (JCPDS Nos. 48-0123, 46-0059, 51-1511). All reflection lines are very broad, indicating the formation of a nanophase [26,27,29,31]. The crystal domain, determined from the FWHM of the (102) diffraction peak using Scherrer's equation after Warren's correction of instrumental broadening [28], is in the range of 7.9–10.5 nm (samples X2).

3.3. Temperature-programmed reduction

TPR was carried out from room temperature to 800 °C under flowing H_2/Ar to obtain relevant information for optimizing the reducing pretreatment conditions. Fig. 4 shows the H_2-TPR profiles of samples X2 (Li2–Cs2) leached twice. A similar trend was observed with all samples. All H_2-TPR curves in Fig. 4 show two main peaks at 300–380 and 500–600 °C with some shoulders, indicating a multistep reduction. The reduction process started at a relatively low temperature (≈180 °C). Careful quantitative analysis of H_2 consumption indicates that the complete reduction of B metals ended around 620 °C. In agreement with results reported previously [26], this suggests that the small shoulder at 200–250 °C can be attributed to the reduction of very small crystallites of CuO. The reduction of intra-framework Cu^{2+} to Cu^0 and Co^{3+} to Co^{2+} was responsible for the signal appearing at around 325 °C. In the presence of alkali chlorides (sample K1), this peak shifted to a higher temperature (∼370 °C), as shown in Fig. 5. This is due to the fact that the reduction of Cu^{2+}/Cu^0 and Co^{3+}/Co^{2+} was somewhat affected by the presence of remnant potassium chloride, in agreement with the observations of Dalmon et al. [16], who reported an increase in the reduction temperature of copper in Al–Co–Cu catalysts with increasing amounts of added Na^+. A similar shift was also observed between samples K2 and K3 (Fig. 5). Moreover, H_2-TPR of sample K3 showed a broader peak at low temperature (240–340 °C) with a detectable shoulder at ∼270 °C, corresponding to the reduction of Cu^{2+}/Cu^0 in perovskites at very low concentration of alkali additives. This is close to the reduction temperature of copper ions in the nonalkalized $LaCoCuO_3$ prepared by reactive grinding reported previously [30]. In contrast, the residual potassium chloride did not affect the reduction of Co^{2+} to Co^0, so that reductions of Cu^{2+} and Co^{2+} were almost resolved in this case [14,16,19,26]. The H_2-TPR profiles of all potassium samples (K1–K3) displayed in Fig. 5 show a higher-temperature peak at 560 °C corresponding to the reduction of Co^{2+} to Co^0. We note that the second reduction stage of Co^{2+}/Co^0 started at 400–620 °C, possibly due to differences in the electronic environment and oxidation state of the cobalt ions [32,33]. The shoulder at 450 °C can be attributed to the reduction of various species of Co^{2+} in the bulk and on the grain boundary (Figs. 4 and 5), whereas the higher peak corresponds to the reduction of cobalt in bulk [29,32]. In addition, the reduction of cobalt ions in Co–Cu-based perovskites always occurs at a lower temperature than that of cobalt in the $LaCoO_3$ [26,30], because the presence of copper in the perovskite lattice strongly promotes cobalt reducibility. Therefore, nanocrystalline $LaCo_{1-x}Cu_xO_{3-\delta}$ perovskites show reduced cobalt at relatively lower temperatures [26,29,30,32]. The H_2-TPR curves suggest optimum pretreatment conditions of 500 °C under flowing hydrogen/argon.

3.4. Catalytic activity

Fig. 6 reports the promotional effect of remnant alkali on the overall catalytic activity in CO conversion at 275 °C. This figure shows that no significant differences in catalytic activity in CO conversion were observed in samples X3 (Li3–Cs3). This indicates that the very small amount of alkali over these samples did not significantly affect the overall activity. The activity data for samples Na3–Cs3 are consistent with that of the nonalkalized $LaCo_{0.7}Cu_{0.3}O_{3\pm\delta}$ sample (57×10^{-3} mmol CO/g_{cat}/h, 275 °C, 1000 psi, 5000 h^{-1}, $S_{BET} = 4.7$ m^2/g) prepared by thermal decomposition of the corresponding amorphous cit-

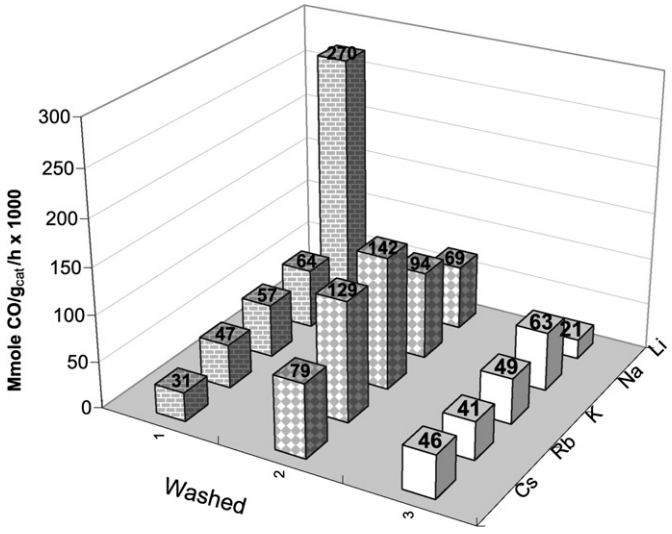

Fig. 6. Effect of residual alkali content on $LaCo_{1-x}Cu_xO_{3-\delta}$ catalytic activity at 275 °C (1000 psi, 5000 h^{-1}, H_2/CO/He = 8/4/3).

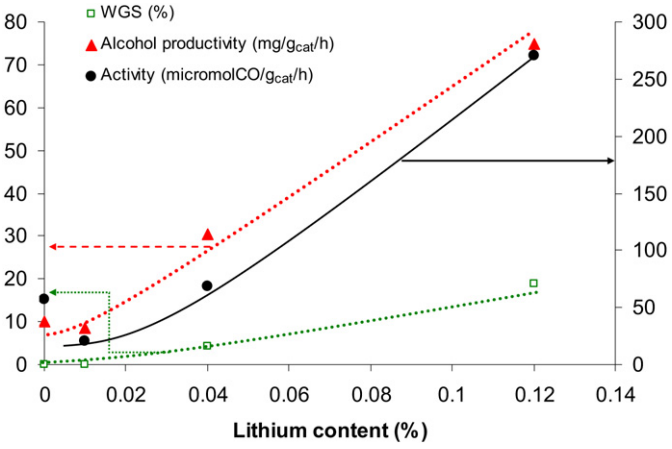

Fig. 7. The correlation between lithium content and the activity in alcohol synthesis at 275 °C (1000 psi, 5000 h^{-1}, H_2/CO/He = 8/4/3; the Li0 content data refer to non-alkalized sample NAl).

rate precursor (not reported in Fig. 6) [1,29]. Therefore, the effect of residual alkali is demonstrated mainly by catalysts X2 and X1. The series of samples Li2–Cs2 showed an irregular variation in the catalytic activity likely associated with the residual amount of alkali (Table 1); samples X1 (Li1–Cs1) exhibited a gradual decrease of CO conversion rate by an order of magnitude from Li (sample Li1) to Cs (sample Cs1). The series of Li-containing catalysts (samples Li1–Li3) exhibited a continuously decreasing CO conversion with decreasing Li content from 0.12 to 0.01 wt%. As shown in Fig. 7, the alcohol productivity in this case was essentially proportional to the Li content, indicating that the remnant lithium acted as a catalytic promoter. In contrast, the data in Fig. 6 for K-, Rb-, and Cs-containing perovskites for each series show maximum CO conversion for samples K2, Rb2, and Cs2. This suggests that in samples K1, Rb1, and Cs1, part of the alkali does not enhance catalytic activity, likely by blocking the access of the reactants to the metal active sites. Partial washing of this alkali resulted

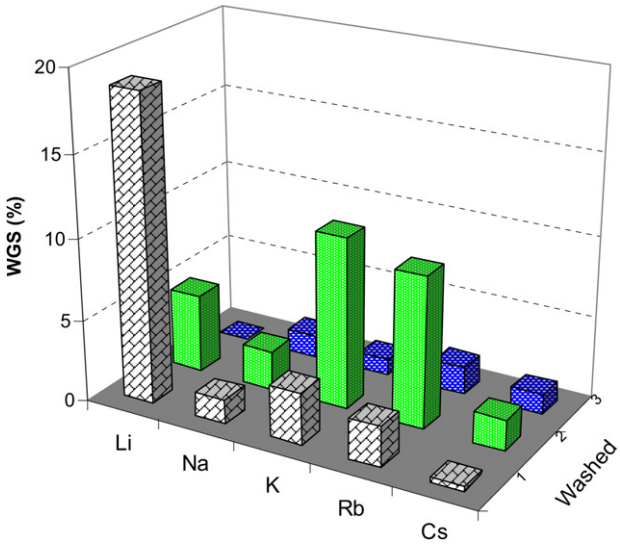

Fig. 8. Effect of residual alkali content on $LaCo_{1-x}Cu_xO_{3-\delta}$ catalytic activity for WGS reaction at 275 °C (1000 psi, 5000 h^{-1}, H_2/CO/He = 8/4/3).

in increased catalytic activity. The Na-containing sample shows an intermediate behavior, with apparent minor changes in activity on washing.

Both higher-alcohol and Fischer–Tropsch syntheses are always accompanied by a reversible WGS reaction [2,3,15,19]. In this study, WGS activity is measured through the CO_2 selectivity, defined as a percentage of CO converted to CO_2. It is assumed that all of the CO_2 results from the WGS reaction,

$$H_2O + CO \leftrightarrow CO_2 + H_2.$$

Fig. 8 shows the CO_2 selectivity over the reduced $LaCo_{0.7}Cu_{0.3}O_{3-\delta}$ perovskites at 275 °C, 1000 psi, VVH = 5000 h^{-1}, and H_2/CO/He = 8/4/3. In combination with Fig. 6, this figure clearly shows that WGS rate is well correlated with overall activity. A high selectivity to CO_2 is observed with all samples Na2–Cs2 along with sample Li1, which retains a lithium content of about 0.12 wt%. Alkali elements are known to be good promoters for the WGS reaction when introduced at optimum content [8,11,12,23,35]. Fig. 8 clearly indicates that in this study, a proper content of remnant alkali over the present perovskite catalysts for the WGS reaction should be close to 0.1–0.3 wt% (samples Li1 and Na2–Cs2). As indicated above, a higher concentration of alkali metals inhibits the WGS reaction by blocking active sites [8,11]. This explains the lower WGS activity observed with samples Na1–Cs1 compared with Na2–Cs2 (see Fig. 8). The lower concentration of alkali promoters on samples X3 is ineffective for WGS reaction, in line with the nonalkalized sample NAl (0.45% CO_2 selectivity) in the conditions reported in Fig. 9.

3.5. Alcohol selectivity and productivity

Table 2 reports the product distribution for CO hydrogenation over the three series of catalysts at 275 °C, 1000 psi, VVH = 5000 h^{-1}, and H_2/CO/He = 8/4/3. The effect of remnant alkali additive content on alcohol productivity is reported in Fig. 9. Comparing Figs. 9 and 6 shows that the trend in al-

Table 2
Product distribution (wt%) at 275 °C, 5000 h^{-1}, 1000 psi (H_2/CO/He = 8/4/3)

Catalyst	Li1	Li2	Li3	Na1	Na2	Na3	K1	K2	K3	Rb1	Rb2	Rb3	Cs1	Cs2	Cs3	NAl
Methanol	7.2	12.0	13.9	15.4	14.8	14.7	11.4	12.7	12.6	11.6	10.9	14.5	11.6	10.4	12.3	6.9
Ethanol	8.2	9.8	11.6	11.2	14.3	14.0	16.2	12.9	11.6	8.6	7.0	13.3	8.9	9.2	11.5	9.6
Propanol	4.7	6.4	6.3	6.5	6.4	6.7	8.4	7.2	6.3	6.1	5.8	6.5	6.6	6.0	6.0	3.2
Butanol	2.9	4.1	3.2	3.9	2.5	2.6	6.1	3.6	2.7	3.0	3.2	2.5	9.8	3.4	2.7	2.7
C_5^+-OH	2.6	4.2	3.3	3.9	2.8	2.9	6.9	3.3	2.8	4.6	4.3	2.8	6.4	4.7	2.9	3.0
C_5^+-olefins	2.5	5.2	2.8	6.8	4.6	3.1	8.4	8.5	4.5	17.2	16.6	5.6	18.7	21.0	5.9	2.0
Methane	29.8	25.8	33.8	23.5	28.3	30.5	18.1	25.5	32.4	22.1	15.8	32.2	11.5	17.2	34.3	41.1
C_2^+ hydrocarbons[a]	44.5	37.7	27.9	32.5	30.9	28.5	33.0	34.8	31.5	43.9	52.9	28.1	45.2	49.1	30.1	31.1
Total alcohols	25.7	36.4	38.1	41.0	40.7	41.0	48.9	39.7	36.2	33.9	31.3	39.5	43.3	33.7	35.4	25.8

Note. NAl: non-alkalized $LaCo_{0.7}Cu_{0.3}O_{3-\delta}$ prepared by citrate complex method, pretreated at 525 °C for 6 h.
[a] Including C_5^+-unsaturated hydrocarbons.

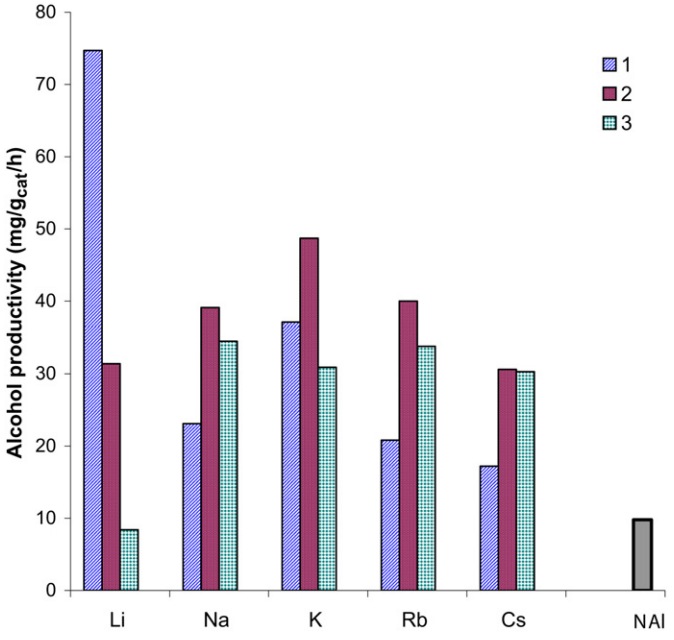

Fig. 9. Effect of residual alkali on alcohol productivity at 275 °C (1000 psi, 5000 h^{-1}, H_2/CO/He = 8/4/3, NAl; non-alkalized sample).

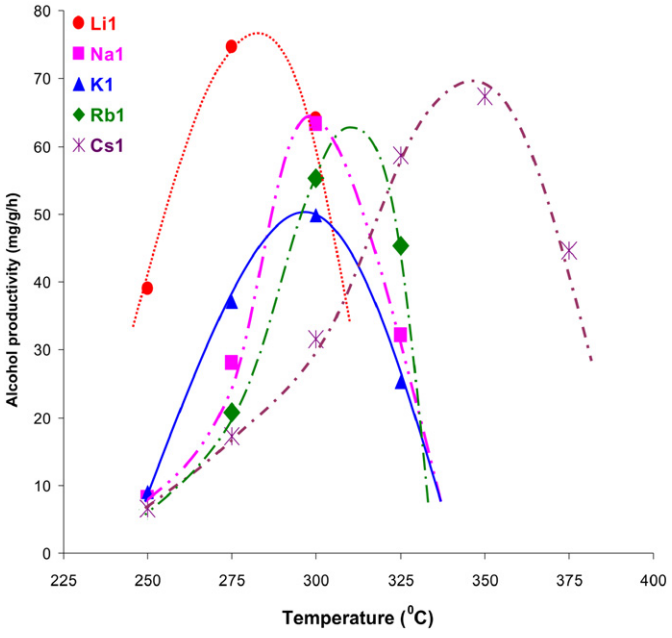

Fig. 10. Alcohol productivity at different reaction temperatures (1000 psi, 5000 h^{-1}, H_2/CO/He = 8/4/3).

cohol productivity varies with the nature of the alkali and that its content is globally similar to that of converted CO. The alcohol productivity over samples Na3–Cs3 is higher than expected, however, closer to that on samples Na2–Cs2. However, the remnant alkali additives in samples X1 and X2 yield a systematically lower selectivity for methane but a higher one for C_2^+-hydrocarbons, implying that the presence of alkali promotes the carbon chain growth probability of products. Nevertheless, as mentioned above, only a very small content of remnant alkali affects the formation of higher alcohols from syngas. Indeed, it was observed that the variation of the rates of CO converted to alcohols and hydrocarbons as a function of alkali content at 275 °C (with the exception of the Li-promoted samples discussed above (Fig. 7) passes through a maximum value around 0.2 wt%. The decline of activity in CO hydrogenation above this value likely corresponds to site blocking by an excess of alkali [7,8,12,22]. Increasing the reaction temperature to 300 °C slightly increased the CO conversion to alcohols and hydrocarbons.

Fig. 10 reports variations in alcohol productivity over the temperature range of 250–375 °C. This figure clearly shows that the maximum conversion rate is shifted toward higher temperatures with increasing ionic radius and electronegativity of the alkali cations.

The trends of olefin productivity as a function of reaction temperature are similar to those of alcohols, as reported in Fig. 11. Except for the Li samples, the olefin productivity increases from the Na catalyst to the Cs catalyst, indicating that formation of such products is dependent on the catalyst surface basicity. In addition, the close resemblance in trends between alcohol (Fig. 10) and olefin productivity (Fig. 11) suggests that both products are formed in parallel on the same active sites [14,18,19].

In contrast to the formation of higher alcohols, the production of paraffins and carbon dioxide both increase sharply with increasing reaction temperature, as shown in Figs. 12 and 13. Methane and CO_2 are favored at higher temperatures, leading to a significant change in product distribution. Indeed, CO_2

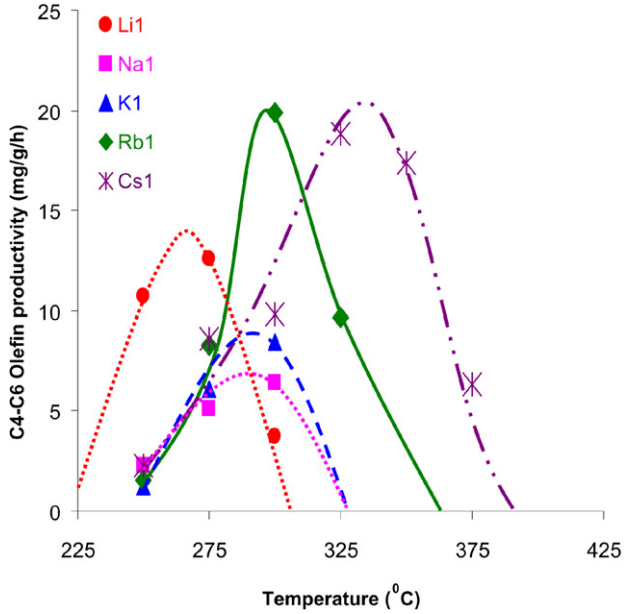

Fig. 11. Olefin productivity at different reaction temperatures (1000 psi, 5000 h^{-1}, H_2/CO/He = 8/4/3).

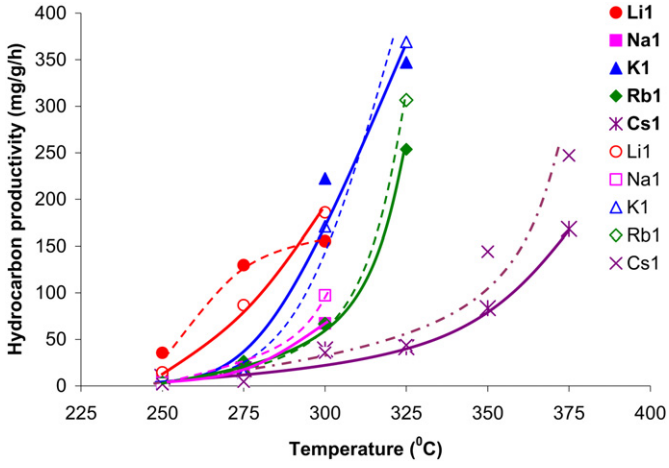

Fig. 12. Hydrocarbon productivity at different reaction temperatures (—: C_2^+-hydrocarbons, – –: methane; 1000 psi, 5000 h^{-1}, H_2/CO/He = 8/4/3).

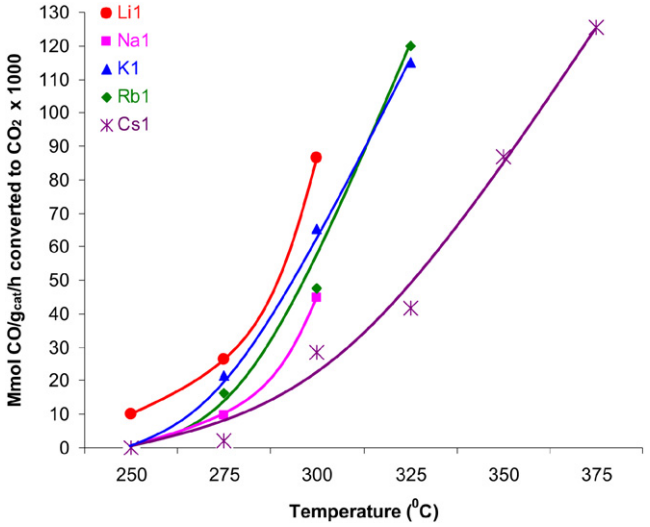

Fig. 13. The rates of CO converted to CO_2 at different reaction temperatures (1000 psi, 5000 h^{-1}, H_2/CO/He = 8/4/3).

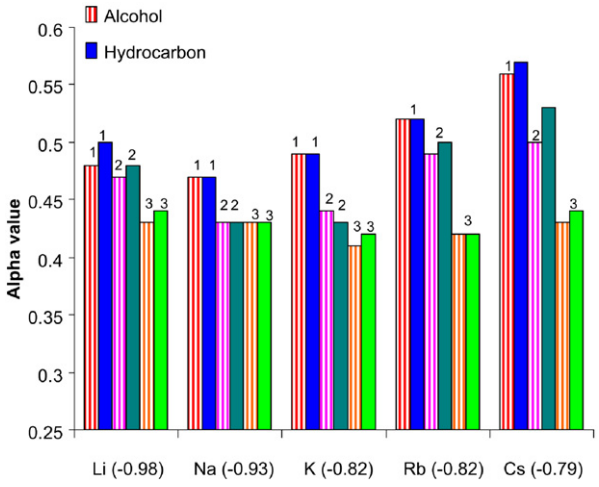

Fig. 14. Effect of alkali promoter on alpha values at 275 °C (1000 psi, 5000 h^{-1}, H_2/CO/He = 8/4/3; the value in parentheses is the alkali electronegativity in eV).

appears to chemisorb on the promoter at the surface of the reduced catalyst and possibly also on the metallic cobalt surface in competition with H_2 and CO reactants [19,24]. Moreover, the significant formation of CO_2 results in a change in the H_2/CO ratio, which directly affects the alcohol formation [19,22]. Obviously, the bell-shaped curves in Figs. 10 and 11 correspond to an activity decreasing at higher temperatures likely associated with a higher rate of desorption of the common intermediate, possibly aggravated by some sintering of the metallic copper [16,23]. Another possible explanation would be related to higher activation energy for hydrogenation than for CO insertion in the carbonaceous intermediate. The latter is supported by the increased hydrocarbon production at increasing temperature (see Fig. 12).

As shown in Figs. 8–12, the alkali promoters not only promote alcohol synthesis, but also enhance catalytic activity in hydrocarbon synthesis and the WGS reaction [7,8,23]. The presence of remnant additives strongly suppresses the formation of methane (Table 2, Fig. 12), possibly due to the decrease in the availability of H* atoms required for termination of growth chains via hydrogen addition reactions to produce paraffins [9,11].

Both normal hydrocarbons and linear alcohols carbon number distributions (measured up to C_{11} for hydrocarbons and C_7 for alcohols) are in good agreement with the ASF distribution. Fig. 14 reports the chain growth probability factors (α) of products at 275 °C over all alkali samples. As reported previously [26], the propagation constants of normal alcohols are very similar to those of hydrocarbons if methanol (even ethanol in some cases) is eliminated from the ASF plot of alcohols. Thus, the alcohol alpha values shown in Fig. 14 are estimated without the addition of methanol (and ethanol in some cases). These chain growth probability factors indeed support the above deductions. Samples Li3–Cs3 give relatively similar value alphas

($\alpha \approx 0.42$) of products, confirming the absence of a significant effect of alkali promoter on the carbon chain growth at this very low content. Samples X1 and X2 show higher alpha values compared with samples X3. Although for all Li catalysts the chain growth probability factors of alcohols are somewhat lower than those of hydrocarbons, these alpha values are still higher than those obtained on samples Li3–Cs3 (Fig. 14) and on the nonalkalized sample NAl ($\alpha_{\text{Alcohol}} = 0.36$). For all samples except Li samples, which always retain a low additive content (Table 1), the propagation constants of both series of products (hydrocarbons and alcohols) are dependent on the electronegativity of the alkali promoter, which was described in a qualitative manner by Pauling as the ability of an atom in a molecule to attract electrons to itself [36]. Fig. 14 displays an increase in chain growth probability factors with the decrease in electronegativity from Na to Cs for the two series of samples X1 and X2. This indicates that the presence of a stronger basic alkali ion on the catalyst surface promotes a longer carbon chain of products [7,37].

4. Discussion

This study has found that introduction of alkali additives into the ground Co–Cu-based perovskites during catalyst synthesis not only affects catalyst morphology, but also has a strong effect on catalytic activity. Moreover, each alkali metal has a different effect on physical and chemical catalytic properties. The catalytic characterization studies (BET, XRD) strongly indicated that after washing, a small amount of alkali remaining over nanocrystalline Cu–Co-based perovskites is finely dispersed on the catalyst surface and/or at the grain boundaries. The H_2-TPR data confirm that the reducibility of perovskite precursors associated with the Co–Cu surface metal is affected by the presence of alkali elements. An interaction between the transition metal sites and basic alkali ions avoids to some extent sintering of the perovskite nanocrystals and disappearance of the grain boundaries also associated with catalyst activity [26,29,30,32]. The reaction test results demonstrate that small fractions of such residual alkali ions act as promoters for CO hydrogenation. The low value of this optimum content (0.2 wt%) is in line with the literature values on methanol, higher-alcohol, and Fischer–Tropsch syntheses, indicating that very low alkali content is sufficient to promote catalytic activity [12,13,15–25,38,39].

The presence of alkali additives accelerates the reaction rates of higher-alcohol production, C_2^+-hydrocarbon synthesis, and WGS reaction in some cases, but inhibit methanation [14,15,38,39]. This is strongly associated with the modification of active sites on the catalyst surface of the reduced $LaCo_{0.7}Cu_{0.3}O_{3-\delta}$ perovskites. When exposed to synthesis gas, metallic cobalt is active in the dissociative adsorption of CO molecules, C–C chain growth, and methane production [17–19]. Nonetheless, suppression of methane formation was seen in samples Li1–Cs1 due to enhanced stability of the CH_x species on the surface with strong basic alkali sites [18,19,40]. As a result, the C–C chain growth would be improved dramatically via CH_x addition, leading to formation of a longer hydrocarbon chain. Furthermore, termination of the hydrocarbon chain was done by either CO insertion into the M–C bond of surface CH_x fragment, followed by hydrogenation to produce higher alcohols, or hydrogenation to yield hydrocarbon products [16–19,40]. Therefore, the hydrocarbon chain growth probability of products (α) was rather high, but the alcohol productivity was still modest on samples X1 under the reaction conditions reported in Fig. 9. This is because an excess of residual alkali covers the metal surface, decreasing available active metal sites on the grain boundaries. After washing twice, the remnant content of additives was about 0.1–0.15 wt%, which gives the highest alcohol productivity and total activity of CO hydrogenation (Figs. 6 and 9).

All alkali metals are able to promote the productions of C_2^+-alkanes, alcohols, and the WGS reaction (Figs. 8–11) [16], but the heavier ones can facilitate olefin formation and suppress methane production [7,38]. This is explained by the fact that the strong basic alkali ions on the catalyst surface prevent the sintering of active metal sites (Co, Cu) on heating and interact strongly with both CO species adsorbed and the alcohol molecule formed [13,15,24,25,37]. In other words, the metal surface area of pretreated perovskite precursors is affected by the presence of a strongly basic alkali ion (K, Rb, Cs) on the surface, as clearly indicated by H_2-TPR results (Fig. 5) [1,5,7]. The appearance of olefin products on samples promoted by alkali suggests that such promoters may affect the hydrogenation function of cobalt sites by an electronic interaction between Co-promoter and inhibits secondary reactions of α-olefins [7,9,37].

The effect of residual alkali over samples X3 on higher-alcohol synthesis is not clear, because of the very small amount of additive retained. Clearly, two successive washings leached almost all alkali elements out of the catalyst precursor, leading to the "liberation" of copper/cobalt sites from a strong interaction between metal sites and alkali promoters and increasing the specific surface area (Fig. 2). Therefore, both copper and cobalt ions in perovskite lattice were reduced at lower temperatures, providing more metallic Co surface. This resulted in increased conversion of CO into light hydrocarbons over samples Li3–Cs3. Consequently, the total selectivity to alcohols gradually decreased and methane selectivity increased from samples X2 to X3. This is in agreement with the results for the nonalkalized sample (NAl), which produced significant methane (>41%) and C_2^+-hydrocarbons (>30%) (Table 2). These observations are consistent with the conclusion of Courty et al. [14], who observed the uncontrolled methanation occurring <290 °C over Cu–Co–Al (IFP) catalysts without alkali promotion [14,16,23].

The alpha values for all promoted catalysts become much meaningful when considering the effect of alkali on carbon chain propagation. There was a gradual decrease in alpha values of alcohols and hydrocarbons from samples X1 to X3. In essence, as shown in Fig. 14, the chain growth probability factor (α) of higher alcohols is similar to that of hydrocarbons, because the carbon skeleton of such products is formed on the same active sites, as proposed previously [14,18,19,26]. However, the chain growth probability factors of hydrocarbons and alcohols increased with decreased alkali electronegativity from Na to Cs (Fig. 14). This indicates that the stronger-basicity al-

kali metal can improve the stability of CH_x intermediate species to prolong the hydrocarbon chain and depress methane formation [9,11,19].

5. Conclusion

Using group I element additives during catalyst preparation resulted in enhanced specific surface area of $LaCo_{1-x}Cu_xO_{3-\delta}$ nanoperovskites. The catalyst surface area increased in the order Li < Na (≈Cs) < K < Rb. After washing with water, the residual amount of alkali additives in the catalysts was in the range of 0.05–0.75 wt%, and the specific surface area of samples calcined at 200 °C ranged from 13.6 to 46.8 m^2/g. Under controlled pretreatment conditions, nanocrystalline $LaCo_{1-x}Cu_xO_{3-\delta}$ perovskites were reduced to produce finely dispersed cobalt copper metals that act as active sites for CO conversion. Residual alkali metals on the catalyst surface affected both perovskite reducibility and the overall activity in syngas conversion. The remnant additives over samples X1 induced decreased methane production, but increased selectivity toward alcohols and C_2^+-hydrocarbons. Samples X2 were most active for CO hydrogenation and yielded the highest alcohol productivity for all alkali additives except Li. The very small amount of residual alkali over samples X3 demonstrates an insignificant effect on alcohol synthesis, as observed with the nonalkalized sample NAl. The role of remnant alkali ions is to promote the carbon chain growth of hydrocarbon and alcohol products. All alkali ions promote the production of alcohols and hydrocarbons but exhibit variable activity in methanation, olefin formation, and the WGS reaction. The optimum reaction temperature is strongly dependent on the nature of the alkali and increases from Li to Cs catalysts.

Both alcohols and hydrocarbon products were consistent with the ASF distributions. The chain growth probability factors were in the range of 0.43–0.57 for both hydrocarbons and alcohols. The propagation constants of products were found to be dependent on the alkali electronegativity. Alcohol selectivity was in the range of 25.7–48.9%. Ethanol and higher alcohols accounted for approximately 60–75 wt% of the alcohols produced. Under the reaction conditions of this study, the highest alcohol productivity was about 74 mg/g/h for lithium-promoted perovskite. Our findings indicate that the presence of alkali promoter is necessary for higher alcohol synthesis from syngas.

Acknowledgments

The authors gratefully acknowledge Nanox Inc. (Québec, Canada) and the Natural Sciences and Engineering Research Council of Canada for financial support. They also thank Nanox Inc. for preparing the perovskite catalysts used in this study.

References

[1] J.A.B. Bourzutschky, N. Homs, A.T. Bell, J. Catal. 124 (1990) 52.
[2] L. Bedel, A.-C. Roger, C. Estournes, A. Kiennemann, Catal. Today 85 (2003) 207.
[3] L. Bedel, A.-C. Roger, J.-L. Rehspringer, Y. Zimmermann, A. Kiennemann, J. Catal. 235 (2005) 279.
[4] M. Crespin, W.K. Hall, J. Catal. 69 (1981) 359.
[5] P.R. Watson, G.A. Somorjai, J. Catal. 74 (1982) 282.
[6] H.C. Woo, I.-S. Nam, J.S. Lee, J.S. Chung, Y.G. Kim, J. Catal. 142 (1993) 672.
[7] G.R. Sheffer, T.S. King, J. Catal. 116 (1989) 488.
[8] W. Ngantsoue-Hoc, Y. Zhang, R.J. O'Brien, Appl. Catal. A 236 (2002) 77.
[9] S. Li, A. Li, S. Krishnamoorthy, E. Iglesia, Catal. Lett. 77 (2001) 197.
[10] D.B. Bukur, D. Mukesh, S.A. Patel, Ind. Eng. Chem. Res. 29 (1990) 194.
[11] W.-D. Mross, Catal. Rev. Sci. Eng. 25 (4) (1983) 591.
[12] M.E. Dry, in: J.R. Anderson, M. Boudart (Eds.), Catalysis: Science and Technology, vol. 1, Springer, Berlin, 1981, p. 155.
[13] M.E. Dry, G.J. Oosthuizen, J. Catal. 11 (1968) 18.
[14] P. Courty, D. Durand, E. Freund, A. Sugier, J. Mol. Catal. 17 (1982) 241.
[15] J.G. Nunan, C.E. Bogdan, K. Klier, K.J. Smith, C.-W. Young, R.G. Herman, J. Catal. 116 (1989) 195.
[16] J.A. Dalmon, P. Chaumette, C. Mirodatos, Catal. Today 15 (1992) 101.
[17] M. Blanchard, H. Derule, P. Canesson, Catal. Lett. 2 (1989) 319.
[18] P. Chaumette, P. Courty, A. Kiennemann, B. Ernst, Top. Catal. 2 (1995) 117.
[19] X. Xiaoding, E.B.M. Doesburg, J.J.F. Scholten, Catal. Today 2 (1987) 125.
[20] E. Tronconi, L. Lietti, P. Forzatti, I. Pasquon, Appl. Catal. 47 (1989) 317.
[21] P. Forzatti, E. Tronconi, I. Pasquon, Catal. Rev. Sci. Eng. 33 (1/2) (1991) 109.
[22] A.M. Hilmen, M. Xu, M.J.L. Gines, E. Iglesia, Appl. Catal. A 169 (1998) 355.
[23] A.D. de Aquino, A.J.G. Cobo, Catal. Today 65 (2001) 209.
[24] M. Xu, M.J.L. Gines, A.-M. Hilmen, B.L. Stephens, E. Iglesia, J. Catal. 171 (1997) 130.
[25] J. Nunan, R.G. Herman, K. Klier, J. Catal. 116 (1989) 222.
[26] N. Tien Thao, H. Alamdari, M.H. Zahedi-Niaki, S. Kaliaguine, Appl. Catal. A 311 (2006) 204.
[27] S. Kaliaguine, A.V. Neste, V. Szabo, J.E. Gallot, M. Bassir, R. Muzychuk, Appl. Catal. A 209 (2001) 345.
[28] H.P. Klug, L.E. Alexander, Procedures for Polycrystalline and Amorphous Materials, John Wiley & Sons, New York/London, 1962.
[29] S. Royer, F. Bérubé, S. Kaliaguine, Appl. Catal. A 282 (2005) 273.
[30] R. Zhang, A. Villanueva, H. Alamdari, S. Kaliaguine, Appl. Catal. B 64 (2006) 220.
[31] T. Ito, Q. Zhang, F. Saito, Powder Technol. 143–144 (2004) 170.
[32] B. Echchahed, H. Alamdari, S. Kaliaguine, Int. J. Chem. React. Eng. 4 (2006) A29.
[33] P. Porta, S.D. Rossi, M. Faticanti, G. Minelli, I. Pettiti, L. Lisi, M. Turco, J. Solid State Chem. 146 (1999) 291.
[34] V. Ramaswamy, P. Awati, A.K. Tyagi, J. Alloys Compd. 364 (2004) 180.
[35] H. Arakawa, A.T. Bell, Ind. Eng. Chem. Process Des. Dev. 22 (1983) 97.
[36] L. Pauling, The Nature of the Chemical Bond, Cornell Univ. Press, Ithaca, NY, 1939, p. 58.
[37] E.V. Albano, Surf. Sci. 141 (1984) 191.
[38] R.A. Dictor, A.T. Bell, J. Catal. 97 (1986) 121.
[39] G.R. Sheffer, T.S. King, Appl. Catal. 44 (1988) 153.
[40] M. Bowker, Catal. Today 15 (1992) 77.